ChemPubSoc Europe

DOI: 10.1002/chem.201504018

CHEMISTRY A European Journal Full Paper

Supramolecular Chemistry |*Hot Paper*|

Iodide Recognition and Sensing in Water by a Halogen-Bonding Ruthenium(II)-Based Rotaxane

Matthew J. Langton,[a] Igor Marques,[b] Sean W. Robinson,[a] Vítor Félix,[b] and Paul D. Beer*[a]

Abstract: The synthesis and anion-recognition properties of the first halogen-bonding rotaxane host to sense anions in water is described. The rotaxane features a halogen-bonding axle component, which is stoppered with water-solubilizing permethylated β-cyclodextrin motifs, and a luminescent tris-(bipyridine)ruthenium(II)-based macrocycle component. ^{1}H NMR anion-binding titrations in D_2O reveal the halogen-bonding rotaxane to bind iodide with high affinity and with selectively over the smaller halide anions and sulfate. The binding affinity trend was explained through molecular dynamics simulations and free-energy calculations. Photo-physical investigations demonstrate the ability of the interlocked halogen-bonding host to sense iodide in water, through enhancement of the macrocycle component's Ru^{II} metal–ligand charge transfer (MLCT) emission.

Introduction

The recognition of anions in water remains a key challenge for the field of anion supramolecular chemistry.[1] Whilst examples of abiotic hosts capable of anion binding in organic solvents are plentiful, receptors that can operate in water—without relying primarily on electrostatics or metal coordination—are relatively rare.[2] Recognition in this highly competitive protic media has predominantly been the domain of highly charged hydrogen-bonding receptors, which are frequently pH-dependent[3] or metal-cation-based systems;[4–6] although some recent progress has been made in exploiting the hydrophobic effect for anion recognition by neutral host species.[7–10] Amongst the plethora of biologically and medically relevant anions, the recognition and sensing of iodide in water is of interest both due to its crucial role in hormone biosynthesis by the thyroid gland[11,12] and its use in contrast media for radiographic imaging applications.[13] Examples of anion hosts capable of sensing iodide by optical methods are scarce,[14–17] and to the best of our knowledge, the use of molecular-anion receptors for the host–guest recognition and sensing of iodide in water is unprecedented.

Halogen bonding (XB), the attractive intermolecular interaction between a polarized halogen atom and a Lewis base,[18] has been employed extensively in the solid state for crystal engineering and functional material synthesis,[19,20] but its use in solution-phase anion recognition remains underdeveloped.[21–25] However, in the past few years, a number of studies have demonstrated that XB anion receptors exhibit superior and contrasting recognition properties in comparison to their hydrogen-bonding (HB) analogues.[26,27] For instance, we very recently reported that XB is remarkably effective for halide-anion binding in water, and results in significantly enhanced recognition in acyclic and rotaxane-based receptors compared to the analogous hydrogen-bonding systems.[28]

It has previously been demonstrated that interlocked molecular architectures, such as rotaxanes and catenanes, which are decorated with convergent hydrogen- or halogen-bond donor motifs, are effective anion hosts,[29] and can also be functionalized with optical reporter groups, such as organic fluorophores,[30,31] transition metals[32–34] or lanthanide cations[35,36] for anion-sensing applications.[37]

Herein, we report the first halogen-bonding host structure for anion sensing in water, in the form of a water-soluble, ruthenium(II)-based [2]rotaxane **1** (Figure 1). ^{1}H NMR anion-binding titrations revealed the ability of the XB-rotaxane to bind iodide in water with high affinity and selectivity, concomitant with an enhancement of the MLCT emission from the Ru^{II} complex of the rotaxane's macrocycle component.

Results and Discussion

Rotaxane receptor design and synthesis

The synthesis of the rotaxane host system is shown in Scheme 1. The permethylated β-cyclodextrin-stoppered axle component features a 3,5-bis-iodotriazole pyridinium bi-den-

[a] *Dr. M. J. Langton, S. W. Robinson, Prof. P. D. Beer*
Department of Chemistry, University of Oxford
Chemistry Research Laboratory, Mansfield Road, Oxford OX1 3TA (UK)
E-mail: paul.beer@chem.ox.ac.uk

[b] *I. Marques, Prof. V. Félix*
Departamento de Química, iBiMED and CICECO
Universidade de Aveiro, 3810-193 Aveiro (Portugal)

Supporting information for this article is available on the WWW under http://dx.doi.org/10.1002/chem.201504018.

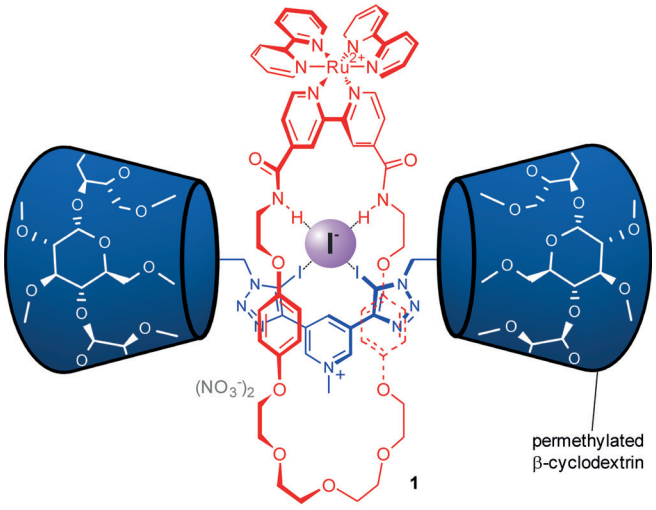

Figure 1. Halogen bonding $[Ru^{II}(bipy)_3]$-based rotaxane **1**.

tate XB-donor motif, which was prepared from 3,5-diethynyl pyridine and the appropriate mono-functionalized azido permethylated β-cyclodextrin derivative using CuAAC "click" chemistry.[28] A 4,4′-bis-amide-2,2′-bipyridyl motif is incorporated into the macrocycle component of the initial precursor rotaxane, to facilitate subsequent metalation with a photo-active $[Ru^{II}(bipy)_2]$ motif. A chloride-anion-templation amide condensation strategy was used for the synthesis of the precursor rotaxane **4**, by stirring the chloride salt of the XB-donor pyridinium axle **2**, bis-amine macrocycle precursor **3**, and 4,4′-bis-(chlorocarbonyl)-2,2′-bipyridine in dry CH_2Cl_2 in the presence of triethylamine.[38] Purification by using preparative silica-gel thin-layer chromatography and size-exclusion chromatography gave the bipyridine-functionalized rotaxane **4** in 40% yield.

NMR and mass-spectrometry techniques were used to fully characterize the rotaxane and confirm its interlocked nature. The ^{1}H NMR spectra of rotaxane **4**, axle **2** and macrocycle precursor **3** are compared in Figure 2. Axle pyridinium protons *a* and *b* are perturbed upfield upon rotaxane formation, whilst the signals corresponding to the hydroquinone protons *4* and *5* of the macrocycle are perturbed upfield and significantly split. This is diagnostic of aromatic donor–acceptor interactions between the electron-rich hydroquinone groups of the macrocycle and the electron-deficient bis-iodotriazole pyridinium π system of the axle component, and is characteristic of interlocked structure formation. Furthermore, cross-peaks observed in the ^{1}H–^{1}H ROESY NMR spectrum revealed multiple through-space interactions between the interlocked macrocycle and axle components, conclusively demonstrating the interlocked nature of the rotaxane product (see Figure S3 in the Supporting Information).

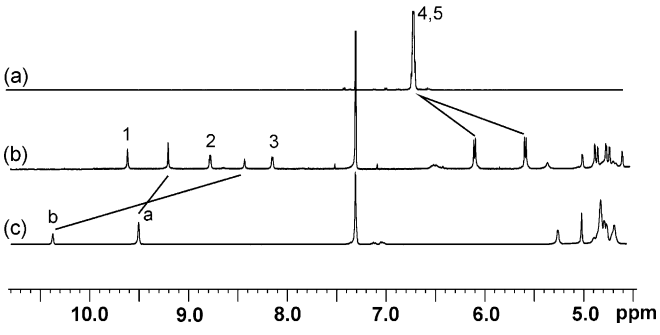

Figure 2. ^{1}H NMR spectra of a) macrocycle precursor **3**; b) rotaxane **4**; and c) axle **2** in $CDCl_3/CD_3OD$ (1:1; 500 MHz). For atom labels, see Scheme 1.

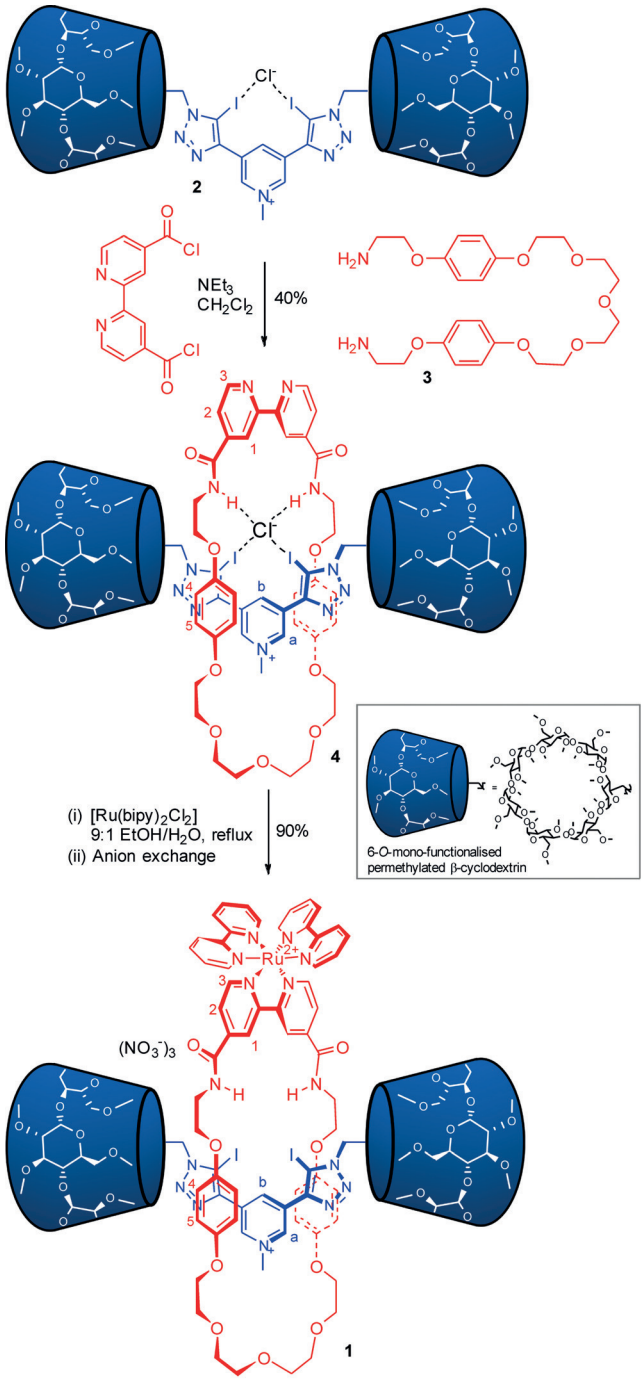

Scheme 1. Synthesis of rotaxane **1** using chloride-anion templation. Inset: schematic representation and chemical structure of 6-*O*-mono-functionalized permethylated β-cyclodextrin.

With the bipyridine-functionalized rotaxane in hand, complexation of the luminescent [$Ru^{II}(bipy)_2$] motif was achieved by heating at reflux rotaxane **4** with [$Ru(bipy)_2Cl_2$] in aqueous ethanol solution to afford the ruthenium XB rotaxane as the chloride salt. This was exchanged to the weakly coordinating nitrate salt—in preparation for aqueous anion-recognition titration experiments—by passing through a nitrate-loaded anion-exchange resin to give rotaxane **1** in 90% yield.

The ruthenium(II)-functionalized rotaxane was fully characterized by using ^1H and ^{13}C NMR spectroscopy and mass spectrometry. The ^1H NMR spectrum of ruthenium rotaxane **1** in D_2O is shown in Figure 3. The hydroquinone protons *4* and *5*

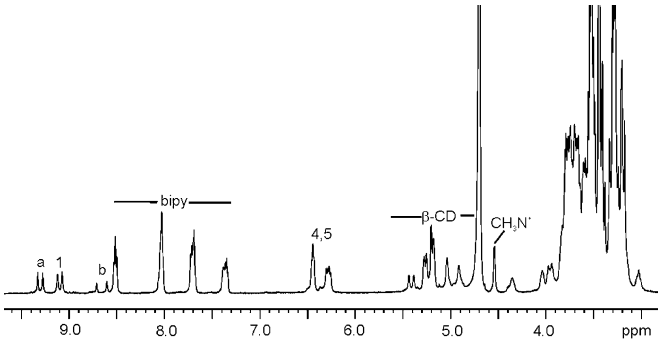

Figure 3. ^1H NMR spectra of rotaxane **1** in D_2O (500 MHz). For atom labels, see Scheme 1.

remain shifted upfield and split, indicating that the interlocked nature of the rotaxane is preserved after the metal complexation, which was further confirmed by analysis of the ^1H–^1H ROESY NMR spectrum (Figure S6 in the Supporting Information). The ^1H NMR spectrum highlights the diasteromeric nature of rotaxane **1**, in which the bipyridine and axle pyridinium protons (*1*, *a* and *b*) are split into two sets of signals of equal intensity.[39]

To facilitate the comparison of the anion-binding properties of the XB ruthenium rotaxane with the respective acyclic, non-interlocked components, a simple water-soluble acyclic ruthenium complex **5**, containing a hydrogen-bond donor 4,4′-bis-amide-2,2′-bipyridyl motif (Figure 4), was also synthesized (see the Supporting Information).

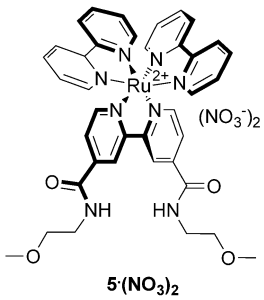

Figure 4. Acyclic hydrogen-bonding ruthenium complex **5**, containing a 4,4′-bis-amide-2,2′-bipyridyl motif for control anion-recognition studies.

We attempted to prepare the hydrogen-bonding analogue to XB-rotaxane **1**, in which the iodotriazole motifs in the axle component are replaced with prototriazole motifs. Unfortunately, rotaxane formation using the same chloride-templation methodology with bis-amine **3**, 4,4′-bis(chlorocarbonyl)-2,2′-bipyridine, and the corresponding 3,5-bis-*proto*triazole pyridinium axle component[28] gave no rotaxane product, and only the non-interlocked axle and macrocycle components were detected by ^1H NMR and ESMS analyses of the reaction mixture.

^1H NMR anion-recognition studies in water

The anion-recognition capability of rotaxane **1** in water was initially studied by ^1H NMR anion-binding titration experiments in D_2O. The sodium salts of various anions were added to a solution of rotaxane **1**, and the chemical-shift perturbations of the protons located within the interlocked cavity binding site (protons *a*, *b* and *1*) were monitored. Addition of halide anions to the rotaxane solution caused a downfield perturbation of the axle pyridinium proton *a*, and upfield perturbations of internal macrocycle bipyridine proton *1* and axle pyridinium proton *b* (depicted for iodide addition in Figure 5 and for other halide

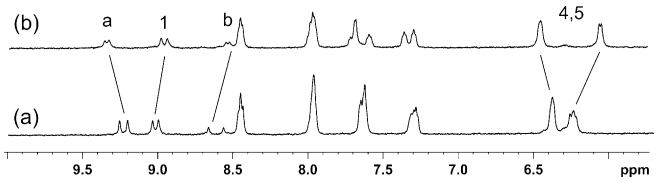

Figure 5. Changes in the ^1H NMR spectrum of rotaxane **1** (D_2O, 500 MHz) upon addition of NaI. a) 0 equiv; b) 1 equiv. For atom labels, see Scheme 1.

anions in the Supporting Information). This is consistent with the halide-anion guest binding within the rotaxane host cavity formed between the interlocked macrocycle and axle components, through convergent XB interactions with the bidentate 3,5-iodotriazole pyridinium motif of the axle, supplemented by hydrogen bonds with the 4,4′-bis-amide-2,2′-bipyridine motif in the macrocycle. Furthermore, the increased splitting of the macrocycle hydroquinone protons *4* and *5* suggest that the rotaxane's geometry is altered to some extent upon iodide binding to accommodate the halide-anion guest. In contrast, addition of sulfate led to a large downfield perturbation of macrocycle bipyridine proton *1*, and no perturbation of pyridinium axle protons *a* and *b* (Figure 6). These contrasting chemical

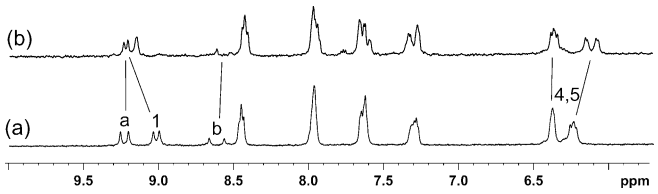

Figure 6. Changes in the ^1H NMR spectrum of rotaxane **1** (D_2O, 500 MHz) upon addition of Na_2SO_4. a) 0 equiv; b) 1 equiv. For atom labels, see Scheme 1.

shift perturbations (compared to those observed with the halide anions) suggest that the sulfate anion is associating on the periphery of the rotaxane, presumably because the oxo anion is too large to penetrate the interlocked binding cavity. Indeed, this hypothesis is supported by molecular dynamics calculations (see below) and similar ^{1}H NMR chemical shift trends were observed for related rotaxane host systems.[28,40,41]

The chemical-shift perturbations of the protons that form part of the anion-binding cavity (protons *1*, *a* and *b* observable throughout the whole course of the titration) were monitored as a function of anion concentration (Figure 7).

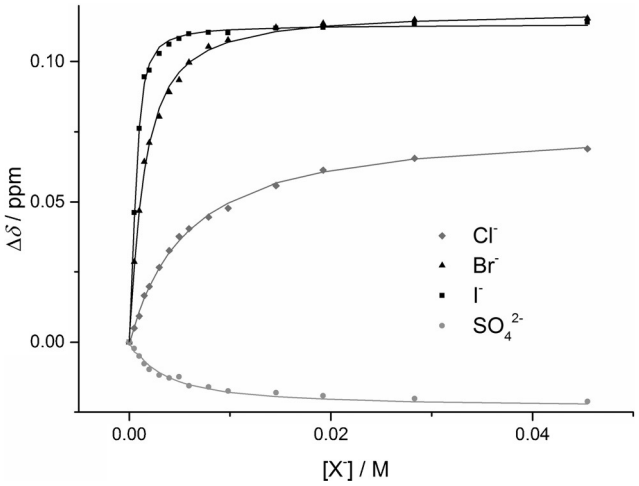

Figure 7. Anion-binding titrations with XB rotaxane **1** (1.5 mM) in D_2O at 298 K. Plots of change in chemical shift of axle pyridinium proton *a* versus anion concentration. For proton assignment, see Scheme 1. Actual data points are represented by solid symbols, and the calculated 1:1 host–guest binding isotherms are represented by solid lines.

WinEQNMR2[41] analysis of the titration data determined the 1:1 stoichiometric association constants shown in Table 1, which for a given anion were consistent for any of the cavity protons monitored. Control titration experiments to determine the anion-recognition capability of the hydrogen-bonding $[Ru^{II}(bipy)_3]$-derived bis-amide complex **5** were conducted in the same way, whilst anion-recognition studies with the corresponding XB acyclic axle component **2** under identical conditions have been previously reported,[28] and are compared in Table 1. The binding of all four anions by the XB rotaxane **1** is of much greater strength than the corresponding acyclic components, **2** and **5**. This effect is consistent with our previously reported rotaxane and catenane anion hosts, in which the combined effects of additional hydrogen-bond donors from the charged macrocycle component, and the creation of a complementary binding domain by mechanically interlocking the components, leads to dramatically enhanced recognition compared to non-interlocked host species.[29]

Table 1. Anion-association constants K_a [M^{-1}] in D_2O.

	Cl^-	Br^-	I^-	SO_4^{2-}
XB rotaxane **1**	190	1020	6300	450
XB acyclic **2**[27]	–*	15	40	–*
HB Ru acyclic **5**	–*	–*	15	35

$T = 298$ K. Anions added as the sodium salt. Association constants determined by ^{1}H NMR anion-binding titrations, using the chemical-shift data of the relevant binding cavity protons (*a*, *b* and *1*). Errors estimated to be $< 10\%$. [*] No binding.

XB rotaxane **1** binds iodide with high affinity in water, with noteworthy selectivity over bromide, chloride and sulfate ($K_a(I^-)/K_a(X^-) = 6$; 33 and 14 for $X^- = Br^-$, Cl^-, and SO_4^{2-}, respectively). By stark contrast, acyclic HB Ru complex **5** is only capable of weakly binding iodide and sulfate with a reverse selectivity trend for the oxo anion (Table 1). The data further supports the hypothesis that the large oxo anion is unable to penetrate the interlocked anion-binding domain, and associates weakly on the rotaxane's periphery. This suggests that the observed selectivity trend for iodide over the smaller halides and sulfate arises from both the intrinsic complementary geometry of the XB rotaxane's binding domain, and the Hofmeister series bias towards the recognition of the larger, less hydrated iodide anion. This is supported by thermodynamic free-energy calculations (see below) conducted on the rotaxane-anion complexes in water.

Importantly, the effect of incorporating halogen-bond donor motifs into interlocked host structural frameworks results in the binding of iodide with remarkably high affinity in water. This effect is consistent with the anion-recognition trend observed for the only other reported water-soluble XB rotaxane host and XB acyclic receptors, in which the incorporation of halogen-bond donors leads to a dramatic enhancement of the anion-binding affinity compared to the analogous hydrogen-bonding species.[28]

Luminescence anion-sensing investigations

The incorporation of the tris(bipyridine)ruthenium(II)-based luminescent motif within the iodide-selective interlocked host framework affords the possibility of sensing this halide anion by means of the modulation of the MLCT emission from the transition metal.[43,44] Such an outer-sphere anion coordination approach (with respect to the ruthenium metal centre) has previously been utilized for halide- and oxo anion-sensing in organic solvents[5] and for the sensing of phosphate[45] and cyanide[46] anions in aqueous media. But to the best of our knowledge, the detection of halide anions in 100% water using this approach has not been reported.

Absorption and emission spectra data for XB ruthenium rotaxane **1** and ruthenium acyclic receptor **5** in water are reported in the Supporting Information. Addition of sodium iodide to a 1×10^{-5} M solution of rotaxane **1** in water gave a three nm hypsochromic shift in the emission wavelength, and reaching a 6% enhancement of the Ru-centred MLCT emission intensity in the presence of excess (1 mM) iodide (Figure S15 in the Supporting Information). This enhancement of emission intensity upon iodide binding is particularly notable because it is more common to observe quenching behaviour of emissive organ-

ic[15–17] or transition-metal-based anion receptors.[47–49] Indeed, in the case of the acyclic HB Ru complex **5**, addition of excess iodide in water caused up to a 10% decrease in the luminescence emission intensity (see the Supporting Information). We postulate that the emission enhancement observed during iodide binding by rotaxane **1** arises from the increased rigidity of the strong iodide rotaxane complex compared to the free rotaxane,[33,50] which reduces the available non-radiative vibrational relaxation pathways that contribute to quenching of the emissive excited state. This process presumably favourably competes with iodide-induced quenching, leading to the observed emission enhancement. Bromide, which binds more weakly, resulted in a smaller enhancement (3%) after the addition of excess anion (1 mM), whereas chloride addition, in contrast, induced no change in the emission spectrum. Addition of sulfate led to larger enhancements of the emission intensity, but only reached its maximum value (20%) in the presence of 8 mM sulfate, thus mirroring the binding selectivity trend determined by NMR titration experiments, which revealed that iodide is bound over an order of magnitude more strongly (see the Supporting Information).[51]

Molecular-dynamics simulations

Following the NMR binding studies, the dynamic behaviour of the anion complexes of XB rotaxane **1** and both the halide anions (Cl^-, Br^- and I^-) and sulfate oxo anion were investigated by means of molecular-dynamics (MD) simulations. These classical force field calculations were carried out with General Amber Force Field (GAFF)[52,53] in periodic boxes of TIP3P water molecules, with the AMBER14 software package.[54] The two putative XB interactions were described with the σ-hole on each axle's iodine atom represented by a positively charged extra point (EP), as was previously reported by us for an analogous XB rotaxane system.[28] The remaining computational details, including the force field parameterization of the tris(bipyridine)ruthenium(II) macrocyclic moiety, as well as the generation of the starting rotaxane anion structures in the gas phase by quenched MD simulations, are given in the Supporting Information.

Four independent MD replicates with production runs of 50 ns were carried out for each XB rotaxane-anion complex, giving a total MD sampling of 200 ns. All four anion complexes exhibit an orthogonal interlocked co-conformation commonly observed for related rotaxane hosts.[40,55] This structure is illustrated in Figure 8 with a selected snapshot taken from a MD run of the iodide complex.

Rotaxane **1** binds each halide anion using two independent XB interactions complemented by two N–H···A (A = Cl^-, Br^- or I^-) hydrogen bonds throughout the MD simulation time. Moreover, both bonding interactions are occasionally interrupted at different simulation times without the complex disruption. The 2D histograms showing the correlation between the I···A distances and C–I···A angles are given in Figure S21 in the Supporting Information, whereas the histograms for the N···A distances versus N–H···A angles are presented in Figure S22 in the Supporting Information.

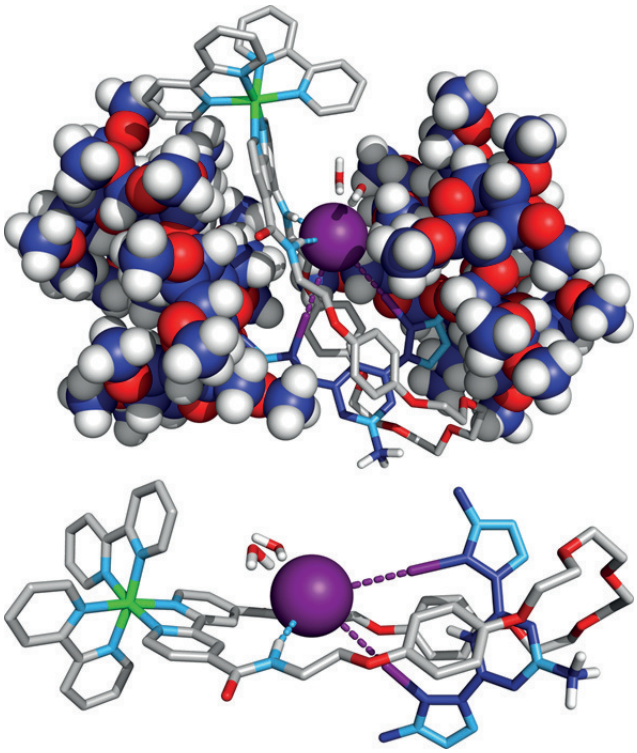

Figure 8. MD representative snapshot of the iodide complex of XB rotaxane **1**. Top: overall structure with the iodide (purple sphere) surrounded by two water molecules and bound by the rotaxane through concomitant XB and HB interactions (purple and light blue dashed lines, respectively). Bottom: further insights into the XB and HB interactions at the binding pocket. The macrocycle and axle are drawn in sticks with carbon atoms in grey and blue, respectively. The oxygen, nitrogen and hydrogen atoms of both rotaxane components are in red, light blue and white, respectively, whereas the ruthenium centre is shown in green. The cyclodextrin stoppers are shown in spheres in the top view, whereas in the bottom view they are omitted for clarity. The NO_3^- counterions are also omitted for clarity.

The plots for the two concomitant XB interactions present well-defined spots, in which a narrow range of distances is also associated with a limited range of angle values, reflecting the highly directional character of these interactions. On the other hand, the HB interactions plots are more scattered, with broader ranges of distance and angle values being monitored, because these interactions are weaker and easier to disrupt along the simulation time. Furthermore, the average N···A and I···A distances listed in Table 2, along with the average angle values of the XB and HB interactions, follow the increasing size of anions. The statistics for the independent replicates are given in Table S2 in the Supporting Information. The halide anions are positioned slightly out of the macrocyclic plane, with average distances of 2.616, 2.839 and 3.044 Å, between Cl^-, Br^- and I^- and the centre of mass of the rotaxane-interlocked binding pocket (defined by the two iodine atoms of the axle and the nitrogen atoms of the macrocycle amide-binding units), respectively. The solvation shells around each anion are characterized by an average number of water molecules at 3.5 Å cut-off from chloride, bromide and iodide of 2.1, 2.5 and 1.8, respectively (Table 2). This demonstrates that the bound halide anion is shielded from the bulk water by the rotaxane

Table 2. Statistics of structural parameters evaluated throughout the 200 ns of sampling of the MD simulations undertaken with anion complexes of **1**.[a]

Anion	Distances [Å] I···A	N···A	$BIND_{COM}$···A_{COM}[b]	Angles [°] C–I···A	N–H···A	Water molecules within 3.5 Å of A
Cl^-	3.533 ± 0.151;	3.687 ± 0.239;	2.616 ± 0.123	173.8 ± 3.2;	159.0 ± 10.9;	2.1 ± 0.7
	3.506 ± 0.147	3.915 ± 0.329		174.0 ± 3.1	151.3 ± 16.3	
Br^-	3.696 ± 0.162;	3.844 ± 0.220;	2.839 ± 0.141	173.8 ± 3.4;	156.1 ± 10.1;	2.5 ± 0.7
	3.691 ± 0.159	3.900 ± 0.261		174.7 ± 2.9	158.9 ± 10.3	
I^-	3.941 ± 0.198;	3.995 ± 0.220;	3.044 ± 0.169	172.6 ± 4.3;	153.6 ± 12.1;	1.8 ± 1.0
	3.941 ± 0.181	4.002 ± 0.257		173.6 ± 3.6	150.6 ± 15.6	
SO_4^{2-}	3.149 ± 0.193;	3.046 ± 0.223;	3.328 ± 0.136	173.0 ± 4.3;	166.1 ± 7.9;	8.5 ± 1.0
	3.098 ± 0.172	3.065 ± 0.188		174.2 ± 3.0	164.5 ± 9.0	

[a] Average ± standard deviations for an $N = 200\,000$ frames. [b] $BIND_{COM}$ stands for the centre of mass of the binding pocket defined by the two nitrogen atoms of the two amide-binding units of the macrocycle and the two iodine atoms of the axle, whereas A_{COM} stands for the centre of mass of the anion in each system.

host's interlocked macrocycle and sterically bulky cyclodextrin stopper axle components.

The selectivity of XB rotaxane **1** for the halide anions in water was further investigated through free-energy calculations, using the thermodynamic integration (TI) method together with standard thermodynamic cycles (illustrated in Figure S26 in the Supporting Information). Alchemic mutations of I^- to Br^- and of Br^- to Cl^- were carried out in water solution, in the presence and in absence of **1** along nine windows, each one with 500 ps of sampling (see the Supporting Information). Throughout this sampling period, the XB and HB interactions in the anion complexes were preserved as requested by the TI approach. The relative binding free energies ($\Delta\Delta G$) were subsequently estimated (see the Supporting Information, Table S5). The two mutations of the free anions are more favourable in water than within the rotaxane host, giving $\Delta\Delta G$ values of 6.01 and 6.55 kcal mol^{-1} for the I^- to Br^- and Br^- to Cl^- transformations, respectively. A third mutation between I^- and Cl^- was also carried out, affording a $\Delta\Delta G$ value of 13.25 kcal mol^{-1}, which differs only 0.70 kcal mol^{-1} from the sum of the I^- to Br^- and Br^- to Cl^- mutation values. This result validates the use of the TI approach to ascertain the $\Delta\Delta G$ values, given that the free energy is a function of state.

The relative free energies indicate that the iodide complex is thermodynamically favoured, followed by the bromide and chloride complexes. Furthermore, this binding preference of rotaxane **1** mirrors the experimentally determined affinity order $I^- > Br^- > Cl^-$, although the theoretical $\Delta\Delta G$ values are overestimated when compared with those calculated from the experimental binding data shown in Table 1.

The putative XB interactions between sulfate and the rotaxane were also simulated through the use of EP as for the halide complexes. However, the use of this approach is not straightforward given that all four oxygen atoms from the oxo anion are able to establish equivalent C–I···O halogen bonds with **1** (see the Supporting Information). A representative snapshot of the four MD replicates is shown in Figure 9. Sulfate recognition occurs through the XB interactions assisted by N–H···O hydrogen bonds with the four oxygen atoms swapping between the axle C–I and macrocyclic N–H binding sites throughout the sampling time. This dynamic behaviour is evident from the histograms built with the I···O and N···O distances presented in Figures S23 and S24 in the Supporting Information. In addition, the larger sulfate anion is positioned above the macrocycle, being further way from the centre of mass of the interlocked binding pocket (3.328 ± 0.136 Å) than any of the smaller monoatomic halides (Table 2), which is in agreement with the ^{1}H NMR titration structural findings.

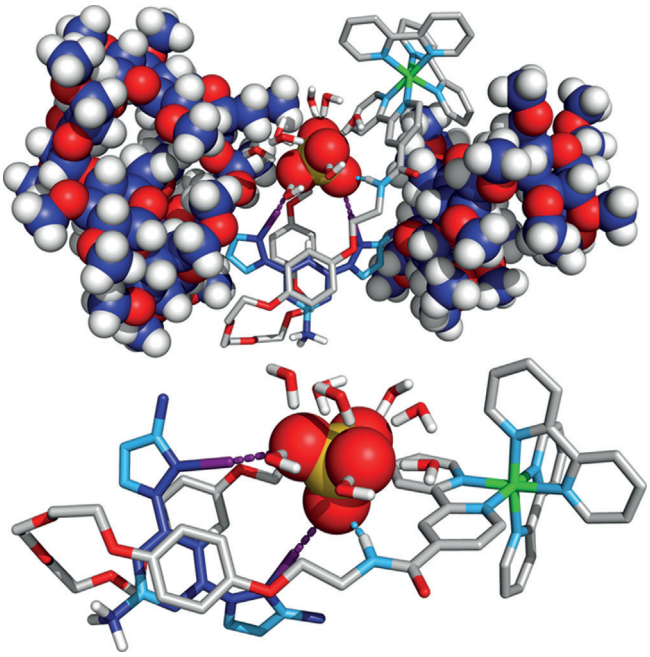

Figure 9. MD representative snapshot of the sulfate complex of rotaxane **1**. Top: overall structure with the sulfate (shown in spheres) surrounded by several water molecules and bonded to the rotaxane interlocked host through concomitant XB and HB interactions. Bottom: further insights into the XB and HB interactions at the binding pocket. The oxygen atoms of the sulfate anion are shown in red, whereas the sulfur atom is shown in yellow. Remaining details as given in Figure 8.

The sulfate anion is also more exposed to solvent with the water molecules at 3.5 Å cut-off ranging between 5 and 13, with an average number of 8.5 ± 1.0. This structural data unambiguously demonstrates that the oxo-anion has a poor fit to the interlocked rotaxane-binding pocket, leading to weak XB

and HB interactions, which is consistent with the association constant value between sulfate and **1** being significantly smaller in magnitude than with iodide, despite the oxo anion's increased charge (Table 1).

Conclusion

The first example of a supramolecular anion host system capable of selectively binding and optically sensing iodide in water has been achieved, by using halogen-bonding interactions within a rotaxane-based receptor to facilitate strong binding of the halide anion guest. A new water-soluble halogen-bonding ruthenium(II) functionalized rotaxane, solubilized with permethylated β-cyclodextrin motifs, was prepared through a chloride-anion templation methodology, and features a tris(bipyridine)ruthenium(II)-based macrocycle component designed for luminescence anion sensing. ^{1}H NMR anion-binding titrations in D_2O revealed strong binding of iodide mediated by convergent halogen- and hydrogen-bonding interactions, with good selectivity over the smaller halides and sulfate. Furthermore, addition of iodide to a solution of the rotaxane in water resulted in enhancement of the Ru^{II} MLCT emission, facilitating the sensing of the anion binding event by luminescence spectroscopy. Structural analyses by MD simulations, together with free-energy calculations, revealed that within the halide series, the selectively of the interlocked host for the iodide anion is dictated by thermodynamic effects, rather than structural ones. In contrast, the sulfate anion, markedly positioned outside the binding pocket, is more exposed to the competitive water solvent molecules, resulting in the relatively low binding for this di-anion with the rotaxane host.

This work represents the first halogen-bonding host capable of sensing anions in pure water, and exemplifies the utility of XB as a superior intermolecular interaction for anion recognition in aqueous solution. The application of halogen bonding in the design of anion sensors capable of operating in water is continuing in our laboratories.

Acknowledgements

M.J.L. thanks the EPSRC for a Doctoral Award and the European Research Council for funding under the European Union's Framework Program (FP7/2007-2013) ERC Advanced Grant Agreement no. 267426. I.M. thanks the FCT for the PhD scholarship SFRH/BD/87520/2012. S.W.R. thanks the Clarendon Fund and St. John's College, Oxford for financial support. The theoretical studies were supported by FEDER through COMPETE and FCT under project UID/BIM/04501/2013.

Keywords: anions · halogen bonding · molecular dynamics · rotaxanes · supramolecular chemistry · water

[1] N. H. Evans, P. D. Beer, *Angew. Chem. Int. Ed.* **2014**, *53*, 11716 – 11754; *Angew. Chem.* **2014**, *126*, 11908 – 11946.
[2] a) S. Kubik, *Chem. Soc. Rev.* **2010**, *39*, 3648 – 3663; b) M. J. Langton, C. J. Serpell, P. D. Beer, *Angew. Chem. Int. Ed.* **2016**, *55*, DOI: 10.1002/anie.201506589; *Angew. Chem.* **2016**, *128*, DOI: 10.1002/ange.201506589.
[3] E. García-España, P. Díaz, J. M. Llinares, A. Bianchi, *Coord. Chem. Rev.* **2006**, *250*, 2952 – 2986.
[4] H. T. Ngo, X. Liu, K. A. Jolliffe, *Chem. Soc. Rev.* **2012**, *41*, 4928.
[5] P. D. Beer, E. J. Hayes, *Coord. Chem. Rev.* **2003**, *240*, 167 – 189.
[6] S. J. Butler, D. Parker, *Chem. Soc. Rev.* **2013**, *42*, 1652 – 1666.
[7] F. Sommer, S. Kubik, *Org. Biomol. Chem.* **2014**, *12*, 8851 – 8860.
[8] M. A. Yawer, V. Havel, V. Sindelar, *Angew. Chem. Int. Ed.* **2015**, *54*, 276 – 279; *Angew. Chem.* **2015**, *127*, 278 – 281; V. Havel, M. A. Yawer, V. Sindelar, *Chem. Commun.* **2015**, *51*, 4666 – 4669.
[9] M. Lisbjerg, B. M. Jessen, B. Rasmussen, B. E. Nielsen, A. Ø. Madsen, M. Pittelkow, *Chem. Sci.* **2014**, *5*, 2647 – 2650.
[10] K. I. Assaf, M. S. Ural, F. Pan, T. Georgiev, S. Simova, K. Rissanen, D. Gabel, W. M. Nau, *Angew. Chem. Int. Ed.* **2015**, *54*, 6852—6856; *Angew. Chem.* **2015**, *127*, 7046 – 7050.
[11] G. Medeiros-Neto, *Thyroid* **1990**, *1*, 73 – 82.
[12] F. Delange, *Thyroid* **1994**, *4*, 107 – 128.
[13] C. M. Rhee, I. Bhan, E. K. Alexander, S. M. Brunelli, *Arch. Intern. Med.* **2012**, *172*, 153 – 159.
[14] H. A. Ho, M. Leclerc, *J. Am. Chem. Soc.* **2003**, *125*, 4412 – 4413.
[15] H. Kim, J. Kang, *Tetrahedron Lett.* **2005**, *46*, 5443 – 5445.
[16] N. Singh, D. O. Jang, *Org. Lett.* **2007**, *9*, 1991 – 1994.
[17] F. Zapata, A. Caballero, N. G. White, T. D. W. Claridge, P. J. Costa, V. Félix, P. D. Beer, *J. Am. Chem. Soc.* **2012**, *134*, 11533 – 11541.
[18] G. R. Desiraju, P. S. Ho, L. Kloo, A. C. Legon, R. Marquardt, P. Metrangolo, P. Politzer, G. Resnati, K. Rissanen, *Pure Appl. Chem.* **2013**, *85*, 1711 – 1713.
[19] P. Metrangolo, F. Meyer, T. Pilati, G. Resnati, G. Terraneo, *Angew. Chem. Int. Ed.* **2008**, *47*, 6114 – 6127; *Angew. Chem.* **2008**, *120*, 6206 – 6220.
[20] L. C. Gilday, S. W. Robinson, T. A. Barendt, M. J. Langton, B. R. Mullaney, P. D. Beer, *Chem. Rev.* **2015**, *115*, 7118 – 7195.
[21] T. M. Beale, M. G. Chudzinski, M. G. Sarwar, M. S. Taylor, *Chem. Soc. Rev.* **2013**, *42*, 1667 – 1680.
[22] A. Mele, P. Metrangolo, H. Neukirch, T. Pilati, G. Resnati, *J. Am. Chem. Soc.* **2005**, *127*, 14972 – 14973.
[23] A. Caballero, F. Zapata, N. G. White, P. J. Costa, V. Félix, P. D. Beer, *Angew. Chem. Int. Ed.* **2012**, *51*, 1876 – 1880; *Angew. Chem.* **2012**, *124*, 1912 – 1916.
[24] S. M. Walter, F. Kniep, L. Rout, F. P. Schmidtchen, E. Herdtweck, S. M. Huber, *J. Am. Chem. Soc.* **2012**, *134*, 8507 – 8512.
[25] S. W. Robinson, C. L. Mustoe, N. G. White, A. Brown, A. L. Thompson, P. Kennepohl, P. D. Beer, *J. Am. Chem. Soc.* **2015**, *137*, 499 – 507.
[26] M. G. Sarwar, B. Dragisic, S. Sagoo, M. S. Taylor, *Angew. Chem. Int. Ed.* **2010**, *49*, 1674 – 1677; *Angew. Chem.* **2010**, *122*, 1718 – 1721.
[27] N. L. Kilah, M. D. Wise, C. J. Serpell, A. L. Thompson, N. G. White, K. E. Christensen, P. D. Beer, *J Am Chem. Soc* **2010**, *132*, 11893 – 11895.
[28] M. J. Langton, S. W. Robinson, I. Marques, V. Félix, P. D. Beer, *Nat. Chem.* **2014**, *6*, 1039 – 1043.
[29] G. T. Spence, P. D. Beer, *Acc. Chem. Res.* **2013**, *46*, 571 – 586.
[30] M. J. Langton, P. D. Beer, *Chem. Eur. J.* **2012**, *18*, 14406 – 14412.
[31] C. G. Collins, E. M. Peck, P. J. Kramer, B. D. Smith, *Chem. Sci.* **2013**, *4*, 2557 – 2563.
[32] D. Curiel, P. D. Beer, *Chem. Commun.* **2005**, 1909 – 1911.
[33] L. M. Hancock, E. Marchi, P. Ceroni, P. D. Beer, *Chem. Eur. J.* **2012**, *18*, 11277 – 11283.
[34] B. R. Mullaney, A. L. Thompson, P. D. Beer, *Angew. Chem. Int. Ed.* **2014**, *53*, 11458 – 11462; *Angew. Chem.* **2014**, *126*, 11642 – 11646.
[35] C. Allain, P. D. Beer, S. Faulkner, M. W. Jones, A. M. Kenwright, N. L. Kilah, R. C. Knighton, T. J. Sørensen, M. Tropiano, *Chem. Sci.* **2012**, *3*, 489 – 493.
[36] M. J. Langton, O. A. Blackburn, T. Lang, S. Faulkner, P. D. Beer, *Angew. Chem. Int. Ed.* **2014**, *53*, 11463 – 11466; *Angew. Chem.* **2014**, *126*, 11647 – 11650.
[37] M. J. Langton, P. D. Beer, *Acc. Chem. Res.* **2014**, *47*, 1935 – 1949.
[38] L. M. Hancock, P. D. Beer, *Chem. Eur. J.* **2009**, *15*, 42 – 44.
[39] We also prepared the [$Re^{I}(CO)_3Cl$]-complexed analogue of XB ruthenium rotaxane **1** (see the Supporting Information, compound S2). Unfortunately, the rotaxane was insoluble in water preventing further study of its anion recognition capability in aqueous solutions.
[40] L. M. Hancock, L. C. Gilday, S. Carvalho, P. J. Costa, V. Félix, C. J. Serpell, N. L. Kilah, P. D. Beer, *Chem. Eur. J.* **2010**, *16*, 13082 – 13094.

[41] M. řezanka, M. J. Langton, P. D. Beer, *Chem. Commun.* **2015**, *51*, 4499 – 4502.
[42] M. J. Hynes, *J. Chem. Soc. Dalton Trans.* **1993**, *2*, 311 – 312.
[43] R. Martínez-Máñez, F. Sancenón, *Chem. Rev.* **2003**, *103*, 4419 – 4476.
[44] K.-C. Chang, S.-S. Sun, M. O. Odago, A. J. Lees, *Coord. Chem. Rev.* **2015**, *284*, 111 – 123.
[45] P. D. Beer, J. Cadman, *New J. Chem.* **1999**, *23*, 347 – 350.
[46] H.-J. Mo, Y. Shen, B.-H. Ye, *Inorg. Chem.* **2012**, *51*, 7174 – 7184.
[47] W. B. Swords, G. Li, G. J. Meyer, *Inorg. Chem.* **2015**, *54*, 4512 – 4519.
[48] H. Li, C. Han, L. Zhang, *J. Mater. Chem.* **2008**, *18*, 4543 – 4548.
[49] C. C. Clark, A. Marton, G. J. Meyer, *Inorg. Chem.* **2005**, *44*, 3383 – 3385.
[50] P. D. Beer, S. W. Dent, T. J. Wear, *J. Chem. Soc. Dalton Trans.* **1996**, 2341 – 2346.
[51] Unfortunately, attempts to obtain quantitative data from the luminescence titration experiments were hampered by the small spectral changes.
[52] J. Wang, R. M. Wolf, J. W. Caldwell, P. A. Kollman, D. A. Case, *J. Comput. Chem.* **2004**, *25*, 1157 – 1174.
[53] J. Wang, R. M. Wolf, J. W. Caldwell, P. A. Kollman, D. A. Case, *J. Comput. Chem.* **2005**, *26*, 114 – 114.
[54] D. A. Case, V. Babin, J. T. Berryman, R. M. Betz, Q. Cai, D. S. Cerutti, T. E. Cheatham, III, T. A. Darden, R. E. Duke, H. Gohlke, A. W. Goetz, S. Gusarov, N. Homeyer, P. Janowski, J. Kaus, I. Kolossváry, A. Kovalenko, T. S. Lee, S. LeGrand, T. Luchko, R. Luo, B. Madej, K. M. Merz, F. Paesani, D. R. Roe, A. Roitberg, C. Sagui, R. Salomon-Ferrer, G. Seabra, C. L. Simmerling, W. Smith, J. Swails, R. C. Walker, J. Wang, R. M. Wolf, X. Wu and P. A. Kollman (2014), *AMBER 14*, University of California, San Francisco.
[55] C. J. Serpell, N. L. Kilah, P. J. Costa, V. Félix, P. D. Beer, *Angew. Chem. Int. Ed.* **2010**, *49*, 5322 – 5326; *Angew. Chem.* **2010**, *122*, 5450 – 5454.

Received: October 7, 2015
Published online on December 2, 2015

